PERGAMON

International Journal of Heat and Mass Transfer 43 (2000) 4285–4297

International Journal of HEAT and MASS TRANSFER

www.elsevier.com/locate/ijhmt

Cylindrical trees of pin fins

M. Almogbel, A. Bejan*

Department of Mechanical Engineering and Materials Science, Box 90300, Duke University, Durham, NC 27708-0300, USA

Received 30 November 1999; received in revised form 2 February 2000

Abstract

In this paper, we extend the constructal optimization method to cylindrical assemblies of pin fins. The assembly is arranged as a tree with one stem and many radial branches. The optimization consists of maximizing the global conductance subject to fixed total volume and amount of fin material. The length scale of the spacing between adjacent elemental fins is selected based on earlier results regarding the forced convection of compact electronic packages. The optimized features of the tree construct are the external shape (height/diameter) and the internal ratio between the stem diameter and the diameter of the elemental fins. The paper shows how the geometric optimum responds to changes in the remaining parameters of the design: the volume fraction occupied by fin material, the free stream velocity, and the Prandtl number. The optimized geometry is relatively robust. It is shown that optimized trees with tapered fins have slightly larger global conductances, but nearly the same external and internal aspect ratios. This last comparison also shows that the more efficient trees look more natural.

1. Introduction

Complex networks of fins are an important class of heat transfer devices in the cooling of electronics and other applications [1–4]. The importance and complexity of these devices promise to increase as miniaturization continues, and as volumetric heat transfer rates increase. The most common fin network is the tree, in which several fins are attached to a stem that makes contact with the wall. This conductive–convective connection between the wall and the cooling fluid is also known as a fin bush or fin tower. Similar fin assemblies are of interest in chemical engineering, entropy generation minimization and fractal geometry [5–7].

The tree is the flow structure that connects one point (source, sink) with a volume (an infinity of points). More recently, this structure has become the focus of *constructal theory* [8] — the thought that the geometric form visible in natural flow systems is generated by (i.e., it can be deduced from) a single principle that holds the rank of law [9]: "for a finite-size system to persist in time, it must evolve in such a way that it provides easier access to the imposed currents that flow through it."

The constructal optimization of paths for internal currents was first proposed in the context of urban growth [10] and pure heat conduction [9]. In the latter, the channels were inserts of high thermal conductivity in a background medium (the interstitial material) that had lower thermal conductivity. The volume generated heat at every point, and was cooled from a single point (the sink). The method was, since, extended to fluid flow [11] by recognizing the heterogeneity associated with low-resistance flow through tubes embedded

* Corresponding author. Tel.: +1-919-660-5310; fax: +1-919-660-8963.

E-mail address: abejan@duke.edu (A. Bejan).

0017-9310/00/$ - see front matter
PII: S0017-9310(00)00049-1

Nomenclature

A	area, m^2	T_1	central stem temperature, K
D	diameter, m	T_∞	free stream temperature, K
h	heat transfer coefficient, W m^{-2} K^{-1}	U	free stream velocity, m s^{-1}
H	length, m	W	length, m
H_1	diameter of first construct, m	V	volume, m^3
k	thermal conductivity, W m^{-1} K^{-1}	V_f	fin volume, m^3
L	length, m		
$m_{0,1}$	fin parameters, m^{-1}, Eqs. (5) and (8)	*Greek symbols*	
n_1	number of fins	ν	kinematic viscosity, m^2 s^{-1}
N	number of cylinders	ϕ	fin volume fraction
Pr	Prandtl number		
q, $\dot{Q}$	heat transfer rate, W	*Subscripts*	
$Re_{D_0,\,L}$	Reynolds numbers, (D_0, L) U/ν	0	elemental volume
Re	Reynolds number, $V^{1/3}U/\nu$	1	first construct
S	spacing, m		
T_b	base temperature, K	*Superscript*	
T_w	wall temperature, K	$\sim$	dimensionless notation, Eqs. (19)–(21)

through a diffusive material with higher resistance (e.g., Darcy flow).

The method was also extended to combined conduction and convection in the optimization of two-dimensional trees of plate fins [12]. The objective of the present paper is to continue on this path, and to consider three-dimensional constructs of cylindrical pin fins (Fig. 1). Unlike in the fin-tree studies mentioned in the preceding paragraphs, the focus of the present paper is on geometric optimization, not on analysis. We rely on simplifying assumptions. We are interested in a simple and robust method that leads not only to

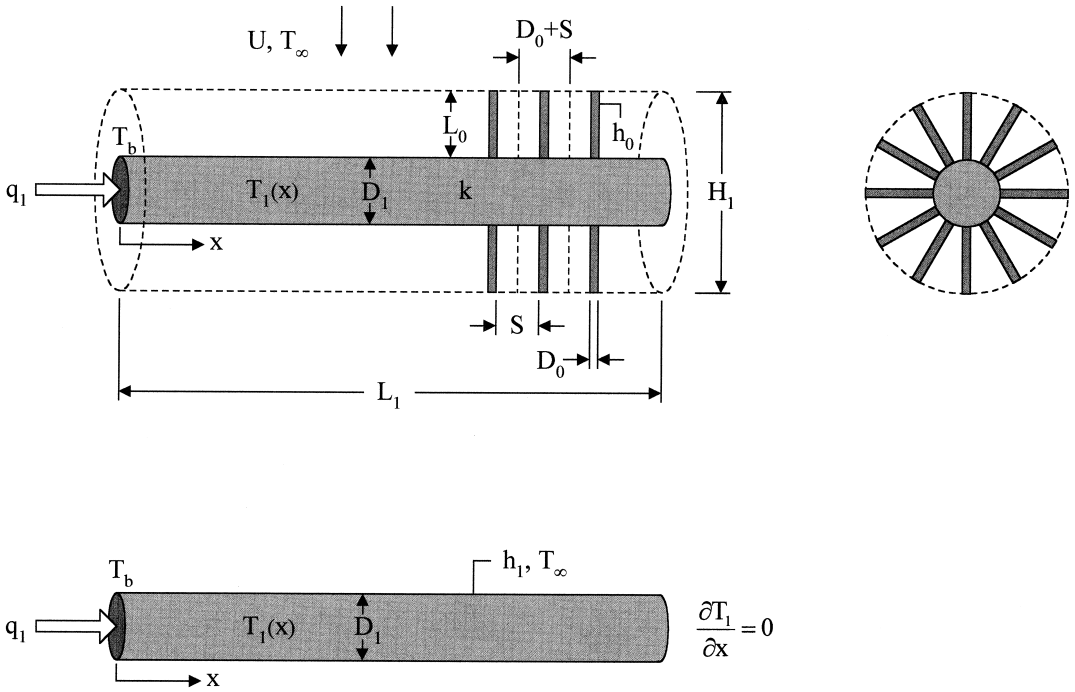

Fig. 1. Cylindrical assembly of radial pin fins bathed by a free stream.

the optimal architecture of the point-to-volume heat path, but also the existence of the fin tree as the visible component of that path.

2. Model and analysis

Consider the assembly of pin fins shown in Fig. 1. A large number (n_1) of pin fins is mounted radially on a common cylindrical stem of length L_1 and diameter D_1. The free ends of the pin fins describe a cylindrical surface of diameter H_1. Each pin fin has the diameter D_0 and length L_0. This assembly is a "first construct" in the sense of Ref. [9], such that the space allocated to a single pin fin plays the role of elemental volume.

If S is the spacing between adjacent pin fins (Fig. 1, detail), we may approximate each elemental volume as a cylinder of diameter ($D_0 + S$):

$$V_0 = \frac{\pi}{4}(D_0 + S)^2 L_0 \tag{1}$$

This statement is approximate because, in general, two adjacent pin fins are not parallel: they are closer at the root than at the tip. The spacing S is an average (effective) length scale that accounts for the actual spacing that increases in the radial direction, away from the D_1 stem. The correct scale of S follows from the requirement that the sum of the elemental volumes (1) must equal the annular volume that surrounds the D_1 stem

$$\frac{\pi}{4}\left(H_1^2 - D_1^2\right)L_1 = n_1 V_0 \tag{2}$$

Another relation of geometric compatibility between the elemental volumes and the first-construct external dimension H_1 is

$$H_1 = 2L_0 + D_1 \tag{3}$$

The assembly transfers heat from a base-wall of temperature T_b to a free stream of velocity U and temperature T_∞ (Fig. 1). The base heat current (q_1) is divided into n_1 elemental currents (q_0), which are later transferred by convection to the fluid. We assume that the direct convective heat transfer between the D_1 stem and the fluid is negligible relative to the n_1 conduction heat currents that flow into the elemental pin fins. We also assume that the conduction along the D_1 stem and the D_0 pins conforms to the unidirectional model [1]: we monitored the validity of this assumption by checking the Biot number inequality $hD_0/k \ll 1$.

Let $T_1(x)$ be the local temperature of the D_1 stem, i.e. the base temperature of the pin fin(s) situated at the distance x away from the base T_b. The heat current drawn from the stem by each pin fin is [13]

$$q_0 = (T_1 - T_\infty)\left(k\frac{\pi}{4}D_0^2 h_0 \pi D_0\right)^{1/2} \tanh(m_0 L_0) \tag{4}$$

where k is the thermal conductivity of the fin material, h_0 is the heat transfer coefficient between the pin fin and the external stream, and m_0 is the fin parameter

$$m_0 = \left(\frac{4h_0}{kD_0}\right)^{1/2} \tag{5}$$

According to the simplest fin conduction model, Eq. (4) is based on the assumptions that (i) h_0 does not vary with position, and (ii) the heat transfer through the free end of the pin fin is negligible. Assumption (i) does not mean that h_0 is a fixed parameter: we will see in Eq. (32) that h_0 varies with the spacing S, which can be chosen optimally [14]. Assumption (ii) was made only for the sake of brevity in the writing of Eq. (4), in order to show explicitly what parameters influence the value of q_0. For the numerical results developed in Section 4, we used the complete q_0 expression for a fin with non-negligible heat transfer through the tip; e.g., Eq. (41).

The final step in the heat transfer analysis is the relation between the overall conductance $q_1/(T_b - T_\infty)$ and the cooling effect provided by the elemental heat currents of type q_0. This step is simplified considerably by the observation that although q_0 varies along the D_1 stream, each elemental conductance $q_0/(T_1 - T_\infty)$ is independent of the axial position x. The heat transfer rate removed by pin fins from the D_1 stem at x = constant, per unit length of stem, is $q' = (n_1/L_1)q_0$. Dividing q' by the perimeter of contact (πD_1) and the temperature difference between the stem and the external fluid ($T_1 - T_\infty$), we obtain an x-independent parameter:

$$h_1 = \frac{(n_1/L_1)q_0}{\pi D_1 (T_1 - T_\infty)} \tag{6}$$

Parameter h_1 plays the same role as the convective heat transfer coefficient in the case where the D_1 stem is bare and exposed directly to the stream. We rely on this analogy to invoke one more time the formula (4) for the base heat transfer rate through a cylindrical fin with insulated tip, this time for the D_1 stem:

$$q_1 = (T_b - T_\infty)\left(k\frac{\pi}{4}D_1^2 h_1 \pi D_1\right)^{1/2} \tanh(m_1 L_1) \tag{7}$$

$$m_1 = \left(\frac{4h_1}{kD_1}\right)^{1/2} \tag{8}$$

The objective is to determine the optimal architecture of the assembly such that the overall conductance $q_1/(T_b - T_\infty)$ is maximal. This geometric optimization is subjected to two constraints, namely, the total volume

of the assembly

$$V_1 = \frac{\pi}{4} H_1^2 L_1 \quad \text{(constant)} \tag{9}$$

and the amount of fin material,

$$V_f = \frac{\pi}{4} D_1^2 L_1 + n_1 \frac{\pi}{4} D_0^2 L_0 \quad \text{(constant)} \tag{10}$$

An alternative to constraint (10) is the volume fraction (ϕ) occupied by the solid, which is a specified design parameter:

$$\phi = V_f / V \quad \text{(constant)} \tag{11}$$

In preparation for the numerical implementation of this analytical formulation, it is useful to nondimensionalize the equations by using $V_1^{1/3}$ as length scale. The nondimensional counterparts to Eqs. (1)–(9) and (11) are, in order

$$\left(\tilde{H}_1^2 - \tilde{D}_1^2\right)\tilde{L}_1 = n_1 \left(\tilde{D}_0 + \tilde{S}\right)^2 \tilde{L}_0 \tag{12}$$

$$\tilde{H}_1 = 2\tilde{L}_0 + \tilde{D}_1 \tag{13}$$

$$\tilde{q}_0 = \frac{\pi}{2} \tilde{D}_0^{3/2} \tilde{h}_0^{1/2} \tanh\left(2\tilde{L}_0 \tilde{h}_0^{1/2} \tilde{D}_0^{-1/2}\right) \tag{14}$$

$$\tilde{h}_1 = \frac{n_1 \tilde{q}_0}{\pi \tilde{D}_1 \tilde{L}_1} \tag{15}$$

$$\tilde{q}_1 = \frac{\pi}{2} \tilde{D}_1^{3/2} \tilde{h}_1^{1/2} \tanh\left(2\tilde{L}_1 \tilde{h}_1^{1/2} \tilde{D}_1^{-1/2}\right) \tag{16}$$

$$\tilde{H}_1^2 \tilde{L}_1 = 4/\pi \tag{17}$$

$$\phi = \frac{\tilde{D}_1^2 \tilde{L}_1 + n_1 \tilde{D}_0^2 \tilde{L}_0}{\tilde{H}_1^2 \tilde{L}_1} \tag{18}$$

with the following notation

$$\left(\tilde{D}_0, \tilde{L}_0, \tilde{S}, \tilde{D}_1, \tilde{L}_1, \tilde{H}_1\right) = \frac{(D_0, L_0, S, D_1, L_1, H_1)}{V_1^{1/3}} \tag{19}$$

$$\tilde{q}_0 = \frac{q_0}{(T_1 - T_\infty) k V_1^{1/3}} \qquad \tilde{q}_1 = \frac{q_1}{(T_b - T_\infty) k V_1^{1/3}} \tag{20}$$

$$\tilde{h}_0 = \frac{h_0 V_1^{1/3}}{k} \qquad \tilde{h}_1 = \frac{h_1 V_1^{1/3}}{k} \tag{21}$$

The system of seven equations (12)–(18) contains 11 unknowns: $\tilde{D}_0$, $\tilde{L}_0$, $\tilde{S}$, $\tilde{D}_1$, $\tilde{L}_1$, $\tilde{H}_1$, n_1, $\tilde{h}_0$, $\tilde{h}_1$, $\tilde{q}_0$, and $\tilde{q}_1$. One way to structure the optimization is to assume that the heat transfer coefficient $\tilde{h}_0$ is also a specified "external" parameter, that accounts for the velocity and thermophysical properties of the fluid stream. This approach is analogous to what is usually done in analyses of single fins, e.g., Eqs. (4) and (7). In this case the number of unknowns would be 10, and the geometry of the assembly would have 3 degrees of freedom. We did not follow this route, for the reasons given in the next section.

3. Optimal internal spacings

The main objection to assuming that $\tilde{h}_0$ can be specified a priori is that, inside the assembly, the heat transfer coefficient on each pin fin is influenced by the neighboring fins. Recent work [15,16] on the single-phase cooling of arrays of heat-generating components (e.g., electronics) and compact heat exchangers has shown that the overall thermal conductance between a stream of coolant and the volume that contains the array can be maximized by choosing the proper spacing between components, or the proper number of components to be installed in the given volume. An optimal spacing exists because in one extreme (small spacings) the coolant cannot flow easily through the array,while in the other extreme (large spacings) the contact area for heat transfer to the coolant is not sufficient.

By recognizing this trade off at this early stage, we can optimize the $\tilde{S}$ value and the corresponding $\tilde{h}_0$ value, accounting in this way for the fact that in any real assembly the heat transfer coefficient depends on internal dimensions and relative positions. The $\tilde{S}$ and $\tilde{h}_0$ information provided by this preliminary step reduces the number of remaining degrees of freedom to two, cf. the last paragraph of the preceding section.

The literature on optimal internal spacings [15] reports many concrete results, which depend on the assumed shape and orientation of each heat-generating component in the array. The optimal-spacing formulas appear different at first, but they convey the same message. For example, when the array consists of many parallel cylinders of diameter D_0 installed in a fixed volume with the dimension H in the direction of the stream of coolant, the optimal cylinder-to-cylinder spacing is given by [17]

$$\frac{S_{opt}}{D_0} \cong 1.7\, Pr^{-0.24} \left(\frac{H}{D_0}\right)^{0.52} Re_{D_0}^{-0.26} \tag{22}$$

This correlation is backed by a large volume of heat transfer information collected from many decades of heat exchanger development and by recent numerical and experimental results. Eq. (22) was shown to be

valid in the range $140 < Re_{D_0} < 14{,}000$, where $Re_{D_0} = UD_0/\nu$.

A more recent study [14] showed numerically and experimentally that an optimal spacing also emerges when the flow is three-dimensional, as in an array of pin fins planted on a square base of side L, with the flow (U) impinging perpendicularly on that base. The optimal spacing is correlated within 16% by the expression

$$\frac{S_{\text{opt}}}{L} \cong 0.81 Pr^{-0.25} Re_L^{-0.32} \tag{23}$$

which was tested in the range $0.06 < D_0/L < 0.14$, $0.28 < W/L < 0.56$, $0.72 < Pr < 7$, $10 < Re_{D_0} < 700$ and $90 < Re_L < 6{,}000$. The pin fin cross-section was a square with the side D_0. The pin length was W.

The interesting and very useful aspect of the apparently different correlations (22) and (23) is that they contain nearly the same information. Eq. (23) can be rewritten as

$$\frac{S_{\text{opt}}}{D_0} \cong 0.81\ Pr^{-0.25}\left(\frac{L}{D_0}\right)^{0.68} Re_L^{-0.32} \tag{24}$$

which comes surprisingly close to Eq. (22), qualitatively and quantitatively, in spite of the three-dimensional flow pattern and square shape of each pin. The dimension L of the square base of the array with impinging flow, Eq. (24), plays the role of the swept length H of the array with parallel cylinders in cross-flow, Eq. (22).

The geometry of present assembly (Fig. 1) has features in common with the two configurations covered by Eqs. (22) and (24). The flow through the D_0 fins is two-dimensional: it is similar to cross-flow near the fins that are close to the perpendicular to the approach velocity U, and similar to impinging flow near the fins that point toward the approaching stream. In choosing between Eqs. (22) and (24), we retain Eq. (22) because it is supported by a much larger body of heat exchanger data, and because its domain of tested validity is considerably wider. With reference to the dimensions and orientation of the present cylindrical assembly (Fig. 1), we use H_1 in place of H in Eq. (22), and nondimensionalize all the lengths in accordance with Eq. (19):

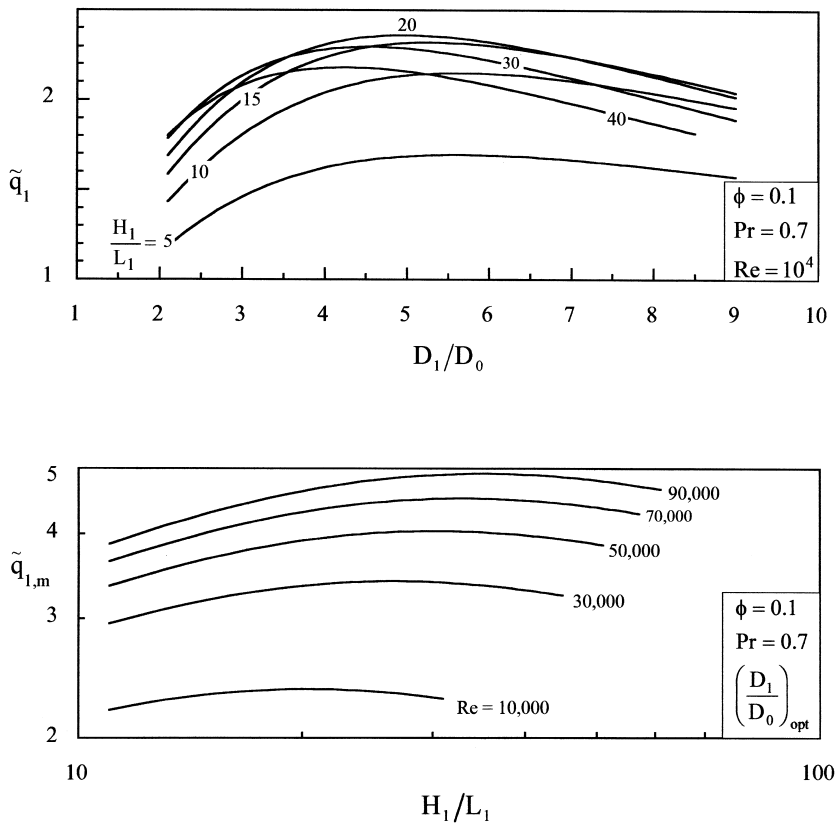

Fig. 2. The maximization of the global thermal conductance with respect to the internal and external aspect ratios of the assembly.

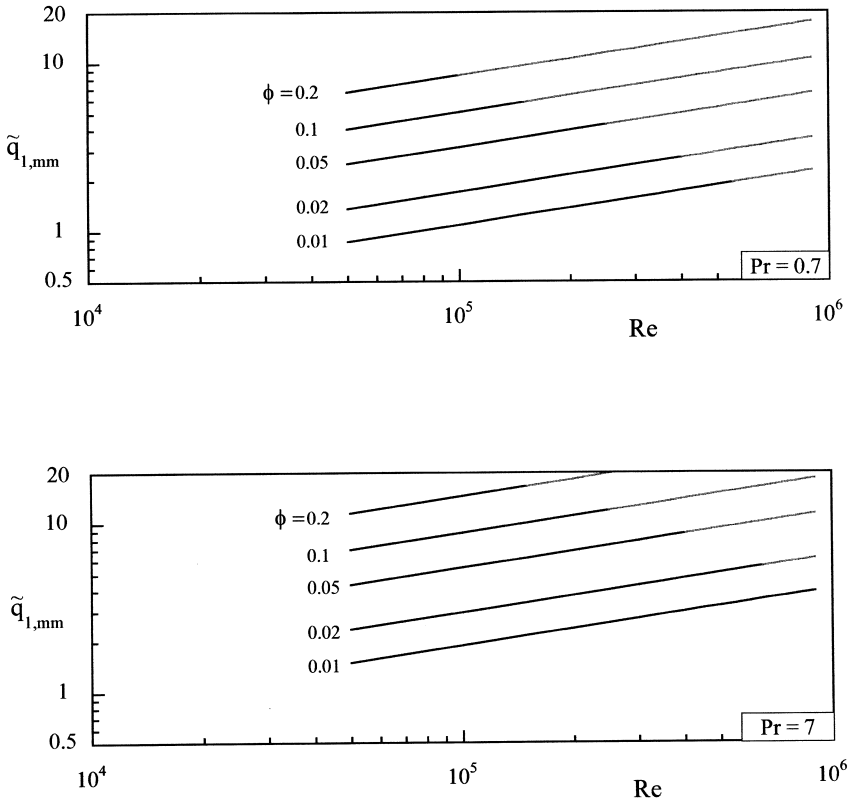

Fig. 3. The maximized global thermal conductance, and the effect of changing ϕ, Re and Pr.

$$\tilde{S} \cong 1.7 Pr^{-0.24} Re^{-0.26} \tilde{H}_1^{0.52} \tilde{D}_0^{-0.22} \tag{25}$$

The Reynolds number Re is now a specified parameter, because it is based on $V_1^{1/3}$ as length scale,

$$Re = UV_1^{1/3}/\nu \quad \text{(constant)} \tag{26}$$

The relation between Re and Re_{D_0} is $Re_{D_0} = \tilde{D}_0 Re$. The specified Re value must be such that the validity domain listed under Eq. (22) is respected,

$$\left(140/\tilde{D}_0\right) < Re < \left(14{,}000/\tilde{D}_0\right) \tag{27}$$

Next, we turn our attention to the heat transfer coefficient $\tilde{h}_0$ that corresponds to the optimal spacing and flow conditions mentioned in Eq. (25). The minimized global resistance between the array of cylinders in cross-flow has been correlated with the formula [17]

$$\frac{T_w - T_\infty}{\dot{Q}} \cong \frac{4.5}{Re_{D_0}^{0.9} Pr^{0.64}} \frac{D_0}{kLW} \tag{28}$$

The cylinder temperature is T_w. The array occupies the fixed volume HLW, where H is the dimension aligned with the stream (U), W is the length of each D_0 cylinder, and L is the second dimension perpendicular to the stream (i.e., the frontal cross-section of the array is LW). We may rewrite Eq. (28) in terms of the array-averaged heat transfer coefficient h_0, which is defined by

$$h_0 = \frac{\dot{Q}}{A(T_w - T_\infty)} \tag{29}$$

The total area for heat transfer is

$$A = N\pi D_0 W \tag{30}$$

where N is the number of cylinders present in the volume HLW. When the cylinder centers form equilateral triangles, as in the arrays for which the correlation (28) was developed, that number is

$$N = \frac{HL}{(S + D_0)^2 \cos 30^\circ} \tag{31}$$

Combining Eqs. (28)–(31), and using the dimensionless notation (19) and (21) with $\tilde{H} = \tilde{H}_1$, we obtain

$$\tilde{h}_0 \cong 0.0613 Pr^{0.64}\, Re^{0.9} \frac{\left(\tilde{S} + \tilde{D}_0\right)^2}{\tilde{H}_1 \tilde{D}_0^{1.1}} \tag{32}$$

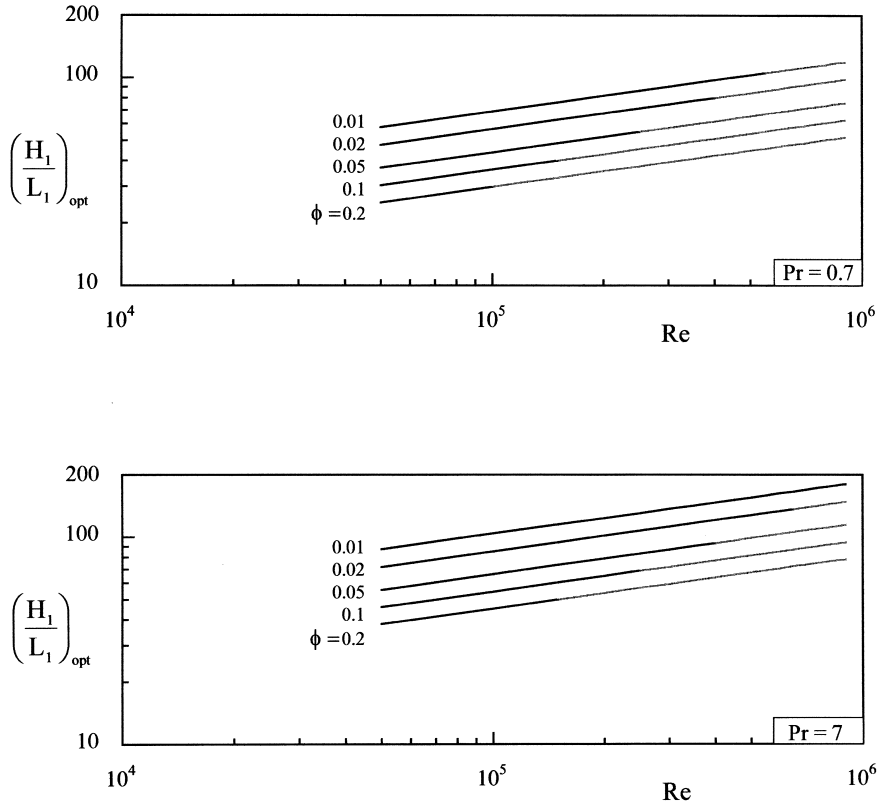

Fig. 4. The optimized external aspect ratio of the cylindrical assembly.

In summary, the heat transfer performance of the cylindrical assembly is described by a system of nine equations [namely, Eqs. (12)–(18), (25) and (32)], that contain the 11 unknowns listed under Eq. (21). This means that the constrained geometry of the assembly has two degrees of freedom. The earlier work on tree networks for pure conduction showed that the overall conductance of the assembly can be maximized with respect to the external shape of the assembly (H_1/L_1 in Fig. 1) and the ratio of internal channel thicknesses (D_1/D_0 in Fig. 1). The same behavior was observed in the present study. In the numerical optimization of the assembly geometry we minimized $\tilde{q}_1$ with respect to H_1/L_1 and D_1/D_0 subject to fixed ϕ and Re.

4. Numerical optimization

Let x and y represent the two independent geometric variables, $x = H_1/L_1$ and $y = D_1/D_0$. The governing equations can be rearranged so that we may calculate the remaining variables as functions of x, y, ϕ and Re:

$$\tilde{H}_1 = (4x/\pi)^{1/3} \qquad \tilde{L}_1 = \tilde{H}_1/x \tag{33, 34}$$

$$\tilde{D}_1^{3.22} - \frac{1.18(\phi-1)Pr^{0.24}\,Re^{0.26}}{\pi\tilde{L}_1 y^{1.22}\tilde{H}_1^{0.52}}\tilde{D}_1^{2.44} + \frac{0.85y^{1.22}\tilde{H}_1^{0.52}}{Pr^{0.24}Re^{0.26}}\tilde{D}_1^{2} - \frac{4\phi}{\pi\tilde{L}_1}\tilde{D}_1^{1.22} - \frac{3.4\phi\, y^{1.22}\tilde{H}_1^{0.52}}{\pi\tilde{L}_1\, Pr^{0.24}Re^{0.26}} = 0 \tag{35}$$

$$\tilde{D}_0 = \tilde{D}_1/y \qquad \tilde{L}_0 = \frac{1}{2}\left(\tilde{H}_1 - \tilde{D}_1\right) \tag{36, 37}$$

$$n_1 = \left(\frac{8\phi}{\pi\tilde{D}_1^2} - 2\tilde{L}_1\right)\frac{y^2}{\tilde{H}_1 - \tilde{D}_1} \tag{38}$$

$$\tilde{S} = \frac{1.7\tilde{H}_1^{0.52}y^{0.22}}{Pr^{0.24}Re^{0.26}\tilde{D}_1^{0.22}} \tag{39}$$

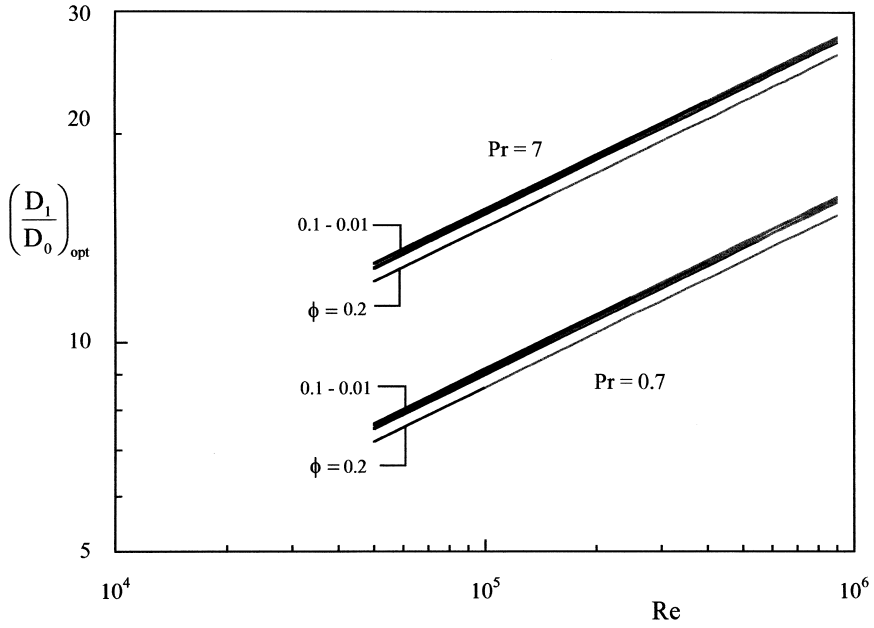

Fig. 5. The optimized ratio of fin thicknesses.

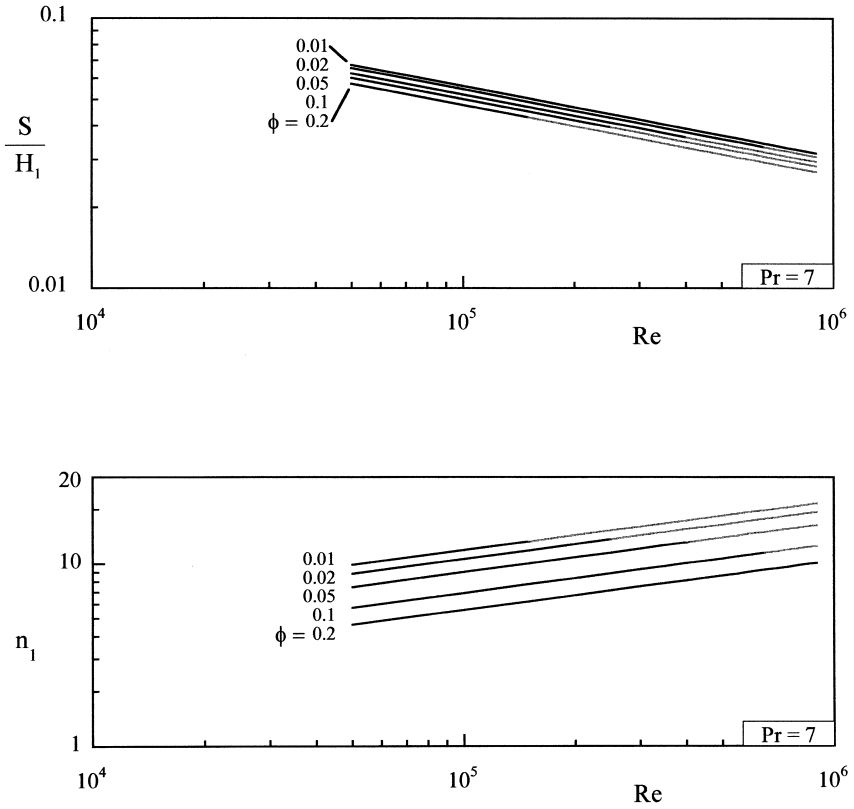

Fig. 6. The average spacing between elemental fins, and the number of elemental fins that corresponds to the optimized geometry of Figs. 3–5.

$$\tilde{h}_0 = 0.0613 Pr^{0.64} Re^{0.9} \frac{\left(\tilde{S}+\tilde{D}_0\right)^2}{\tilde{H}_1 \tilde{D}_0^{1.1}} \tag{40}$$

$$\tilde{q}_0 = \frac{\pi}{2}\tilde{D}_0^{3/2}\tilde{h}_0^{1/2}\left[\frac{\left(\tilde{h}_0\tilde{D}_0/4\right)^{1/2}+\tanh\left(2\tilde{h}_0^{1/2}\tilde{L}_0/\tilde{D}_0^{1/2}\right)}{1+\left(\tilde{h}_0\tilde{D}_0/4\right)^{1/2}\tanh\left(2\tilde{h}_0^{1/2}\tilde{L}_0/\tilde{D}_0^{1/2}\right)}\right] \tag{41}$$

$$\tilde{h}_1 = n_1\tilde{q}_0/\left(\pi\tilde{D}_1\tilde{L}_1\right) \tag{42}$$

$$\tilde{q}_1 = \frac{\pi}{2}\tilde{D}_1^{3/2}\tilde{h}_1^{1/2}\tanh\left(2\tilde{L}_1\tilde{h}_1^{1/2}/\tilde{D}_1^{1/2}\right) \tag{43}$$

The nonlinear Eq. (35) was combined with Eq. (36) and solved for $\tilde{D}_1$ and $\tilde{D}_0$. The numerical procedure was based on the Newton–Raphson method with By-section Technique. The variables were determined in the sequence represented by Eqs. (33)–(43).

In the first phase of the optimization we varied y ($= D_1/D_0$) and maximized the global thermal conductance $\tilde{q}_1$. This phase is illustrated in the upper frame of Fig. 2 for the case $\phi = 0.1$, $Re = 10^4$ and $Pr = 0.7$. The result is recorded as $\tilde{q}_{1,\,m}$, in the lower frame, where the subscript "m" indicates that $\tilde{q}_1$ has been maximized once. We repeated this procedure for many values of $x(= H_1/L_1)$ until we achieved the second maximization of the global conductance. The lower frame of Fig. 2 shows a second, well defined maximum with respect to the external aspect ratio of the cylindrical assembly.

5. Results

The double maximization of $\tilde{q}_1$ was repeated for many combinations of ϕ and Re, which covered the domain $0.01 \le \phi \le 0.2$ and $10^4 < Re < 10^6$. The results are condensed in Figs. 3–6. The twice-maximized conductance $\tilde{q}_{1,\,mm}$ (Fig. 3) increases as the solid volume fraction ϕ and the external Reynolds number Re increase. These trends are expected: more fin material and a faster flow enhance the transfer of heat in a constrained volume. Each curve exhibits a change in darkness at a point that corresponds to the upper limit of the Re range indicated in Eq. (27). The solid black

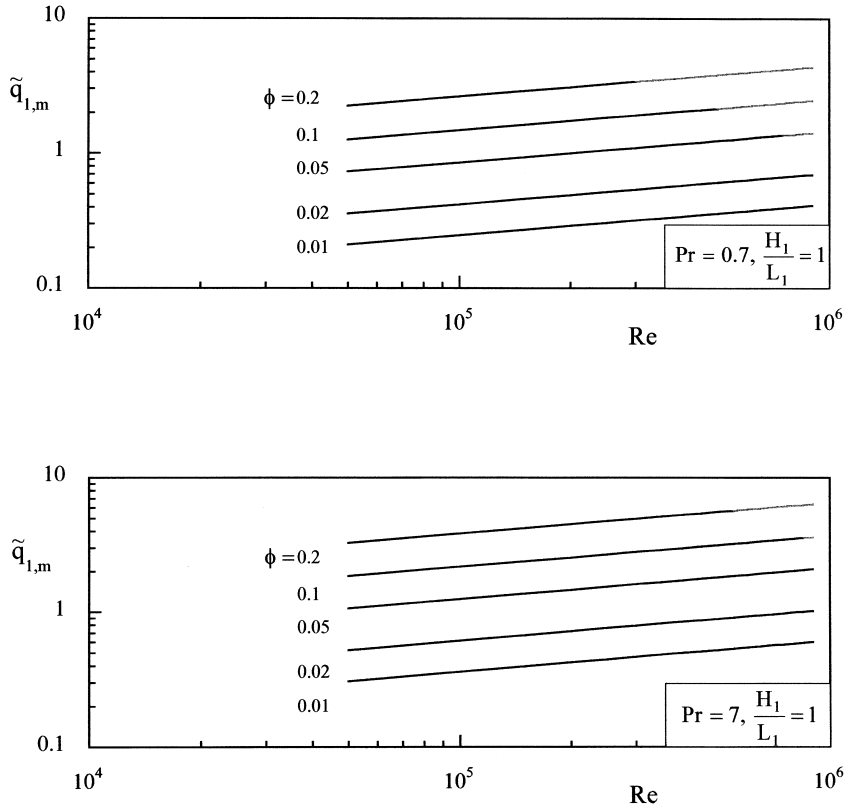

Fig. 7. The maximized global thermal conductance when the external shape is set at $H_1/L_1 = 1$.

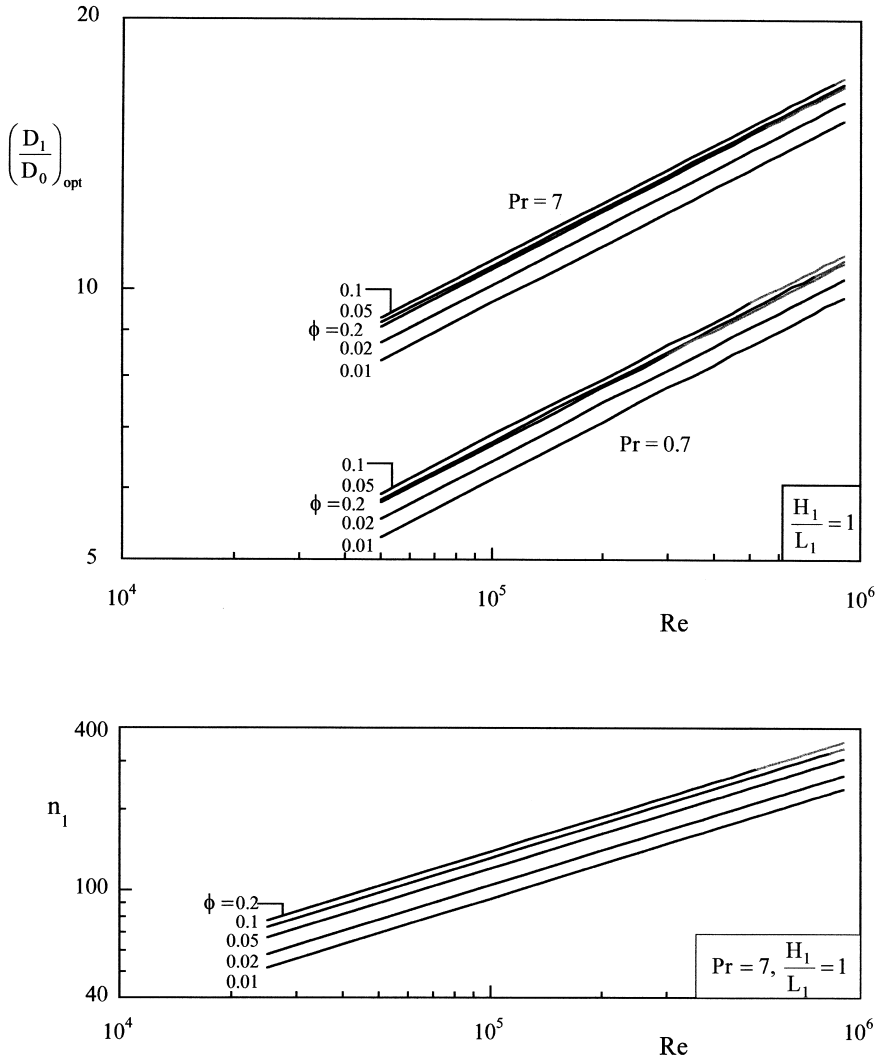

Fig. 8. The optimized ratio of fin thicknesses and the corresponding number of elemental fins when the external shape is set at $H_1/L_1 = 1$.

portion of the curve are for *Re* values in agreement with Eq. (27), i.e., in the range where $\tilde{S}$ correlation (22) and (25) has been tested.

The next figures document the optimized architecture of the assembly, for designs where the global conductance has been maximized twice, in accordance with Figs. 1–3. The optimized external aspect ratio $(H_1/L_1)_{opt}$ is shown in Fig. 4. This ratio decreases as ϕ increases, and is relatively insensitive to the external flow (*Re*). The numerical values of H_1/L_1 are considerably greater than 1, which makes them somewhat incompatible with the model envisaged in Fig. 1. To this observation we return in Section 6. The optimized external dimensions of the assembly can be calculated by combining $(H_1/L_1)_{opt}$ with the volume constraint. For example, the diameter is given by

$$\tilde{H}_1 = \left(\frac{4}{\pi}\frac{\tilde{H}_1}{\tilde{L}_1}\right)^{1/3} \tag{44}$$

The ratio of fin thicknesses $(D_1/D_0)_{opt}$ is relatively insensitive to the solid volume fraction and the Prandtl number (Fig. 5). The effect of *Re* continues to be weak. The values of $(D_1/D_0)_{opt}$ are of order 10, and, combined with the values of $(H_1/L_1)_{opt}$ seen earlier, they describe a design with long and thin elemental fins attached to a short and thick stem. The individual thicknesses (D_0, D_1) can be calculated from the ϕ constraint (10) and (11) in combination with the $(D_1/$

$D_0)_{opt}$ result of Fig. 5, and the external dimensions (L_1, L_0) derived (cf. Eqs. (44) and (3)).

Fig. 6 is a summary of other features that accompany the geometry optimized in Figs. 3–5. The top frame shows the average spacing between the elemental fins, as a fraction of the diameter of the assembly. The ratio S/H_1 is smaller than 1/10, and relatively insensitive to ϕ and Re. The spacings are smaller when there is more material, and when the fluid flows faster. The latter is a common feature of all the optimized spacings reported in the electronics cooling literature [15].

The lower frame of Fig. 6 shows the corresponding number of elemental fins: n_1 is of order 10, and increases as Re increases. The earlier conclusions ($H_1/L_1 \approx 10$, $S/H_1 \approx 1/10$), suggest that this relatively small number of elemental fins can be fitted in very few sub-groups (discs) of the type illustrated on the right side of Fig. 1. In other words, instead of the "cylindrical brush" architecture suggested by Fig. 1, the optimized assembly resembles more closely the spokes of a few wheels or umbrellas, all mounted on the same short stem. It is not a coincidence, then, that in an ongoing study of fin assemblies with very few elements (two, four, six) [18], the optimized designs tended toward the umbrella with short stem architecture.

The number of elemental fins (n_1) was monitored during each double optimization run, in order to limit the calculations only to assemblies that are realistic, i.e. structures in which the elemental fins can be fitted without interference. The maximum number of fins that fit in a wheel-shaped subgroup is $\pi D_1/D_0$ in this limit the bases of the elemental fins just touch. The number of sub-groups that can be installed on the L_1 stem is $L_1/(S + D_0)$. In conclusion, the maximum number of elemental fins is $n_{1,\max} = \pi(D_1/D_0)L_1/(S + D_0)$, which according to the optimized results of Figs. 4–6 is a number of order 30: this is larger than the n_1 values plotted in the lower half of Fig. 6, indicating that the optimized elements can be fitted in an assembly. In addition, the $n_{1,\max}$ criterion allowed us to simplify the numerical search for the two maxima (Fig. 2) by searching only in the $n_1 < n_{1,\max}$ domain.

6. Fixed external aspect ratio

Brush-like constructs can be optimized by fixing the external shape of the volume. In this case the optimization has only one degree of freedom: the ratio of diameters. In Figs. 7 and 8 we show the results obtained for the fixed H_1/L_1. The behavior is

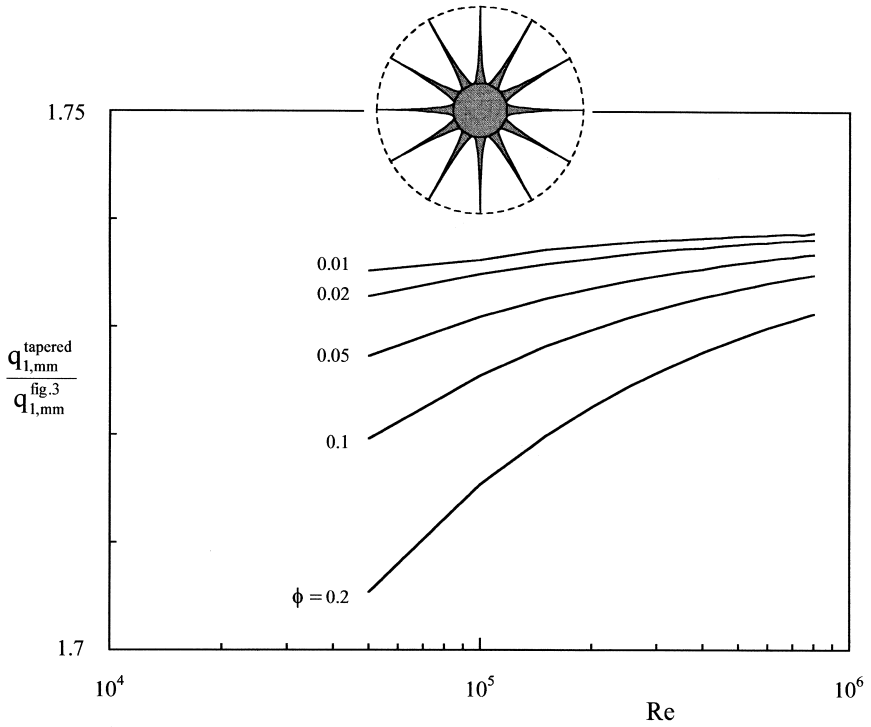

Fig. 9. The increase in global conductance caused by the tapering of the fin profile.

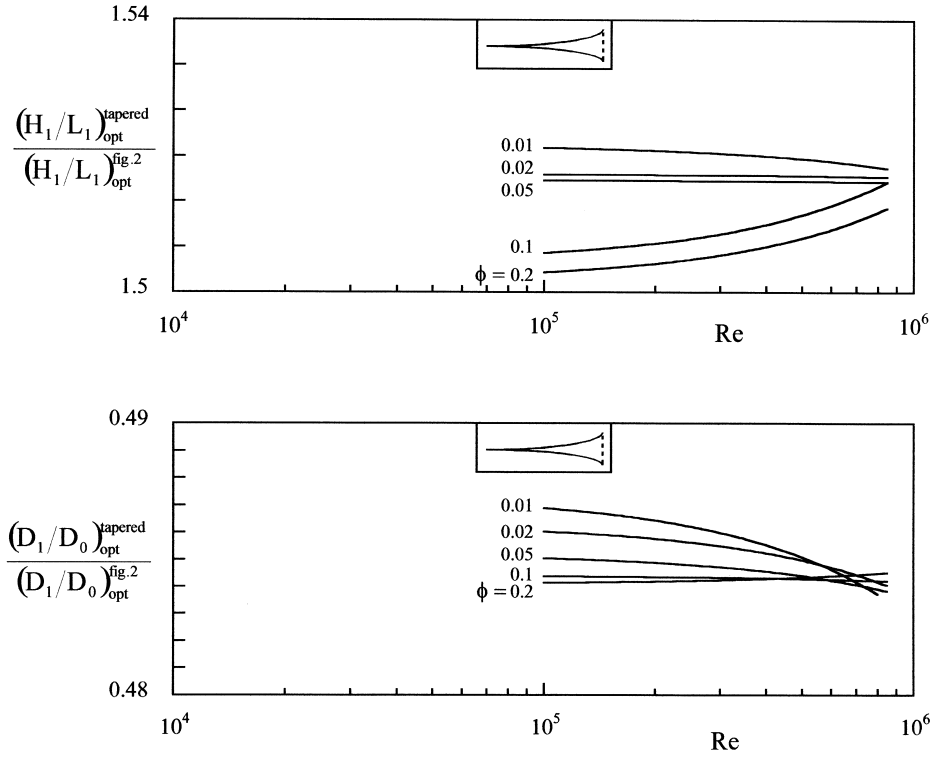

Fig. 10. The relative changes in the external and internal ratios, when the design is changed from constant diameters (Fig. 1) to tapered cylinders.

similar to what we found in Figs. 3, 5 and 6, however, some differences are worth noting.

The maximized conductance (Fig. 7) is lower than in Fig. 3. This comparison shows the relative benefit associated with optimizing the external aspect ratio (Fig. 3), or the penalty associated with using an aspect ratio that is easier to construct (Fig. 7).

The optimized ratio of diameters (Fig. 8, top) is smaller than in Fig. 5, in other words, the distribution of thicknesses is relatively more uniform. The lower part of Fig. 8 shows that the number of elemental fins is of order 100, which is considerably larger than in Fig. 6. Taken together, the results of Figs. 7 and 8 describe an assembly that looks more like a cylindrical brush.

7. Conclusions

In this study we showed that the global maximization of thermal conductance subject to volume and fin material constraints leads to a tree structure in which every geometric detail is derived from principle. In the cylindrical geometry, the parameters derived from optimization are the external aspect ratio of the volume, and the internal ratio between the fin diameters (Fig. 2). The structure is a 'first-construct' with many radial branches distributed on a central stem. We did not continue the method toward constructs of higher order, because the relatively flat cylindrical trees optimized at the first level cannot be grouped smoothly on a new stem, into larger cylindrical volumes.

An important conclusion is the robustness of the optimized geometric features. These features are relatively insensitive to changes in the external parameters imposed on the design. For example, the amount of fin material has almost no effect on the optimized ratio of fin diameters (Figs. 5 and 8). The Prandtl number has a weak effect on geometry. More noticeable is the effect of the free stream velocity (Re): the design shifts toward flatter shapes (larger H_1/L_1) and larger steps in fin diameter as the velocity increases.

The results developed in this paper are orientative in nature, as they are based on several modeling approximations. In addition to the unidirectional conduction model, we adopted results from the geometric optimization of forced convection arrangements [15] in order to select the length scale of the spacing between elemental fins. The correlations for optimal spacings (e.g., Eq. (22)) require further development and testing,

so that their range can be increased. This study shows that a new geometry on which the optimal spacing ideas of Refs. [14–17] can be investigated is the geometry of Fig. 1. One way to start would be to test several designs with different spacings (numbers of fins), using devices with nearly isothermal solid parts.

Even the model employed in this paper can be improved, for example, by abandoning some of the simplifying assumptions made at the start. One assumption is the cylindrical fin of constant diameter. We repeated the study for the case where the elemental cylinder (D_0) is tapered, while maintaining the amount of fin material fixed. This is a classical fin improvement technique [19]. The tapered shape is represented by (Fig. 9 inset) the diameter function $D(x) = D_b(x/L_0)^2$, where x is measured away from the tip, and D_b is the fin diameter at the base. The average diameter is $D_0 = 0.45\ D_b$; this diameter corresponds to the constant-D_0 used in the preceding parts of the paper, that is, when the elemental volume V_0 is the same in both designs. In the tapered-D_0 case the elemental volume is $V_0 = (\pi/20)D_b^2 L_0$.

The effect of this design change is documented in Fig. 9, where the new global conductance is compared with the twice maximized conductance of the constant-diameter design (Fig. 3). The tapering of the fins increases the conductance by a factor of approximately 1.7.

The corresponding geometric features of the tree with tapered elements are documented in Fig. 10, again, with reference to the constant-diameter design. We see that the optimized geometry is nearly the same as in the simpler design with constant diameters. This reinforces the conclusion that the optimized geometry is robust, and that when more degrees of freedom are relaxed (e.g., cylinder diameter) the optimized tree looks more natural.

The designs described in this paper are examples of the more general method of deducing optimal geometric form from a global optimization principle. The thought that the same principle can be used to explain and predict the geometric form (e.g., tree networks) of natural flow systems is constructal theory [8–12]. The applications of this methodology in the optimization of engineering and natural systems are the subject of a new book [20].

Acknowledgements

This work was supported by the National Science Foundation (USA) and the Ministry of Higher Education (Saudi Arabia).

References

[1] A.D. Kraus, A. Bar-Cohen, Design and Analysis of Heat Sinks, Wiley, New York, 1995.
[2] A.D. Kraus, Developments in the analysis of finned arrays, International Journal of Transport Phenomena 1 (1994) 141–164 Donald Q Kern Award Lecture.
[3] A.D. Kraus, Optimization of finned arrays, in: A. Bejan, P. Vadasz, D.G. Kröger (Eds.), Energy and the Environment, Kluwer Academic Publishers, Dordrecht, The Netherlands, 1999, pp. 37–48.
[4] W.R. Hamburgen, Optimal finned heat sinks, in: WRL Research Report 86/4, Digital, Western Research Laboratory, Palo Alto, CA, 1986.
[5] W.W. Lin, D.J. Lee, Diffusion–convection process in a branching fin, Chemical Engineering Communications 158 (1997) 59–70.
[6] D.J. Lee, W.W. Lin, Second-law analysis on a fractal-like fin under crossflow, AIChE Journal 41 (1995) 2314–2317.
[7] W.W. Lin, D.J. Lee, Second-law analysis on a pin-fin array under cross-flow, International Journal of Heat and Mass Transfer 40 (1997) 1937–1945.
[8] A. Bejan, Advanced Engineering Thermodynamics, 2nd ed., Wiley, New York, 1997.
[9] A. Bejan, Constructal-theory network of conducting paths for cooling a heat generating volume, International Journal of Heat and Mass Transfer 40 (1997) 799–816.
[10] A. Bejan, Street network theory of organization in nature, Journal of Advanced Transportation 30 (1996) 85–107.
[11] A. Bejan, M.R. Errera, Deterministic tree networks for fluid flow: geometry for minimal flow resistance between a volume and one point, Fractals 5 (1997) 685–695.
[12] A. Bejan, N. Dan, Constructal trees of convective fins, Journal of Heat Transfer 121 (1999) 675–682.
[13] K.A. Gardner, Efficiency of extended surfaces, Transactions of the ASME 67 (1945) 621–631.
[14] G. Ledezma, A.M. Morega, A. Bejan, Optimal spacing between fins with impinging flow, Journal of Heat Transfer 118 (1996) 570–577.
[15] S.J. Kim, S.W. Lee (Eds.), Air Cooling Technology for Electronic Equipment, CRC Press, Boca Raton, 1996.
[16] S.J. Kim, D. Kim, Forced convection in microstructures for electronic equipment cooling, Journal of Heat Transfer 121 (1999) 639–645.
[17] A. Bejan, The optimal spacing for cylinders in crossflow forced convection, Journal of Heat Transfer 117 (1995) 767–770.
[18] M. Almogbel, Constructal optimization of fin assemblies, Ph.D. Thesis, Duke University, 2000 (in progress).
[19] E. Schmidt, Die Wärmeübertragung durch Rippen, Z. Ver. Dt. Ing. 70 (1926) 885–889 and 947–951.
[20] A. Bejan, Shape and Structure, from Engineering to Nature, Cambridge University Press, Cambridge, UK, 2000.